remote sensing

MDPI

Article

Shifts in Salt Marsh Vegetation Landcover after Debris Flow Deposition

Germán D. Silva *, Dar A. Roberts, Joseph P. McFadden and Jennifer Y. King

Department of Geography, University of California, Santa Barbara, CA 93106-4060, USA; dar@geog.ucsb.edu (D.A.R.); mcfadden@ucsb.edu (J.P.M.); jyking@ucsb.edu (J.Y.K.)
* Correspondence: german.silva@geog.ucsb.edu

Abstract: On 9 January 2018, Carpinteria Salt Marsh Reserve received a large quantity of sediment following debris flows in Montecito, California. Because disturbances potentially impact the ecosystem services and functions that wetlands provide, an understanding of how the ecosystem responded to the debris flows is important for the management of salt marsh systems. However, a lack of field data before and after this disturbance makes this task impossible to complete by field methods alone. To address this gap, we used Sentinel-2 satellite imagery to calculate landcover fractions and spectral indices to produce maps of landcover before, during, and after the debris flow using a random forest classifier. Change detection showed that vegetation extent in November 2020 approached pre-debris flow conditions. While total vegetated area experienced little net change (0.15% decrease), there was a measurable change in the areal extent of vegetation type, with high marsh vegetation transitioning to mid marsh vegetation in regions that initially showed an increase in bare soil cover. These results are uniquely quantifiable using remote sensing techniques and show that disturbance due to debris flows may affect ecosystem function via plant community change. These impacts will need to be taken into consideration when managing wetlands prone to depositional events.

Keywords: remote sensing; wetland change; change detection; random forest classifier; *Salicornia pacifica*

Citation: Silva, G.D.; Roberts, D.A.; McFadden, J.P.; King, J.Y. Shifts in Salt Marsh Vegetation Landcover after Debris Flow Deposition. *Remote Sens.* **2022**, *14*, 2819. https://doi.org/10.3390/rs14122819

Academic Editor: Nicholas Murray

Received: 28 April 2022
Accepted: 7 June 2022
Published: 12 June 2022

1. Introduction

Coastal salt marshes are dynamic ecosystems found at the interface between marine and terrestrial environments. These productive ecosystems play important roles in coastal resilience via a variety of ecosystem services, such as accreting sediments, sequestering carbon, and providing habitat for a rich range of biota [1,2]. However, as little as 10% of California's historical wetland cover remains today [3]. This decrease in wetland cover is likely to worsen with the potential increased frequency of disturbances that further reduce and degrade wetland cover, such as sea level rise, coastal erosion, deposition, and anthropogenic marine debris [4–6]. In Santa Barbara County, CA, a series of large debris flows known as the Montecito Debris Flows exemplify a large-scale depositional disturbance to both built and natural environments, including wetlands. The increasing frequency of events related to climate change, such as fires, hurricanes, and altered hydrology, will likely increase the potential for further debris flows, both locally and globally [7]. To mitigate the impacts of disturbance, management should include the effects of disturbances from debris flows in the understanding of marsh form and function. For instance, sediment deposition is a common and important process in many marshes, with deposition due to hurricanes frequently studied and found to provide sediment important for nutrient delivery and the ability to offset sea level rise [2,5]. In contrast, anthropogenic marine debris, such as fishing gear and wooden poles, has been found to damage plant tissues in marshes [4]; meanwhile, oiling has been found to temporarily increase shoreline loss of affected wetlands [8].

Debris flows are an episodic depositional disturbance event; however, there is little literature studying them in wetlands. Furthermore, many studies examining disturbance

events in salt marshes have focused on the Gulf of Mexico and the east coast of the U.S. [4,5,8–11]. However, the disturbances that are common in those regions, such as hurricanes, are not common on the west coast of the U.S., where debris flows are more common. As such, the question of how the Montecito Debris Flows impacted the marsh is of interest. However, addressing this question with field methods is complicated by the fact that the unpredictability of the event meant that field data could not be collected prior to the event. Furthermore, a combination of manager-led mechanical dredging and inundation by exceptionally high tides, also known as king tides, removed sediment from the marsh and limited the ability to collect field data following the event. Remotely sensed data, however, were collected before and following the event and could be used to assess impacts of the debris flow on the marsh.

Remote sensing has been used for change detection, biomass estimation, and land cover classification in wetlands with a large range of applications [9,12]. Due to recent advances in sensor design and data analysis, remote sensing is becoming more practical for monitoring natural and anthropogenic changes in coastal systems [12]. Prior studies have recommended a variety of sensors (e.g., Landsat, imaging spectrometers, LiDAR, Planetscope, and drone data), techniques (e.g., maximum likelihood classification, Multiple Endmember Spectral Mixture Analysis (MESMA), reclassification, random forest, and post-classification change detection), and indices (e.g., normalized difference vegetation index) to monitor coastal wetland conditions [6,8,9,11,13–17]. Sensor and spectral vegetation index recommendations vary depending on the wetland type and the characteristics that are being assessed. Index recommendations are more dependent on the type of wetland being assessed.

Several approaches have been used to classify land cover in wetlands. One study implemented the use of fractional cover of different endmembers—spectra from pixels that are representative of a land cover, obtained by spectral mixture analysis (SMA) and MESMA [18]—in the classification of a marsh in the southern San Francisco Bay [12]. While both MESMA and SMA have challenges, MESMA was found to provide a more accurate representation of fractional cover, especially if 4- or 5-endmember models were used with more than one endmember per class [12]. Peterson et al. (2015) used MESMA on airborne visual/infra-red imaging spectrometer (AVIRIS) data to detect oil-impacted regions of coastal salt marsh in Barataria Bay, Louisiana with high accuracy of detecting oiled vs. non-oiled marshes (87.5% to 93.3%) [11]. Beland et al. (2017) used these maps and image change analysis to determine that oiling temporarily accelerated land loss in coastal marshes [8]. These studies highlight the effectiveness of MESMA as a technique for classifying wetland landcover and detecting areas affected by disturbance.

Other classification methods have also been used for tracking change. Tuxen et al. (2008) used NDVI to track vegetation colonization in Petaluma River Marsh after tidal restoration via post-classification change detection [19]. They concluded that NDVI can be used to discriminate vegetated and non-vegetated portions of marshes and is robust to human interpretations of NDVI [19]. Another study used Breaks For Seasonal and Trend (BFAST) and random forest classification on monthly NDVI products made from Landsat (5, 7, 8) and MODIS/Landsat fill-in images to perform change detection in forested wetlands with a classification accuracy of 92.96% and change detection accuracy of 87.8% [17]. Parihar et al. (2012) used maximum likelihood classification on Landsat MSS and TM data to track changes in the East Kolkata Wetlands in the absence of ground data, although the accuracy of this method was between 73.80% and 79.33% [14]. Im et al. (2008) showed that object-based land cover classification with high accuracies (>90%) can be achieved with solely using a high point density LiDAR data [20].

In this study, we use random forest classification and change detection to assess how the Montecito Debris Flows impacted landcover in Carpinteria Salt Marsh Reserve. Our main objectives were: (1) classification of marsh landcover before and after the debris flows, (2) identification of what change in landcover had occurred and possible implications,

(3) identification of important classification variables, and (4) assessment of how accurately random forest classification could map marsh landcover.

2. Materials and Methods

2.1. Event and Site Description

In December 2017, the Thomas Fire burned an area of 1140 km^2 in the Santa Ynez Mountains, making it the largest fire in California's history at the time [21,22]. Following the fire, the burned areas experienced an increased risk of debris flows, and, in early January 2018, a heavy rain event mobilized soils from the burn area and triggered a depositional event known as the Montecito Debris Flows [22]. The debris flows deposited approximately 680,000 m^3 of sediment across urban and natural areas along the Santa Barbara Coast [22]. In addition to at least 3 fatalities, 167 injuries, and 408 damaged homes, the Carpinteria Salt Marsh Reserve, an ecological study reserve operated by the University of California, received a large deposition of sediment.

Carpinteria Salt Marsh Reserve (CSMR), located in Carpinteria, CA (34.4012° N, 119.5379° W), is situated between California Highway 101, downtown Carpinteria, and the Pacific Ocean (Figure 1). The wetland is a heterogeneous landscape made up of 93 hectares of annual and perennial herbs and grasses, transitional upland habitat, water channels, and mud flats [6]. The plant community can be split into two main categories: mid marsh, primarily dominated by *Salicornia pacifica* (formerly *Salicornia virginica*, pickleweed), and high marsh, which is a mix of *Salicornia pacifica*, *Jaumea carnosa* (marsh jaumea), *Distichlis littoralis* (shore grass), *Arthrocnemum subterminale* (Parish's glasswort), *Frankenia salina* (alkali heath), and a few other less abundant species [6,23]. Water inputs come largely from tidal inundation and from water inlets in the eastern portion of the marsh that allow for input from further inland [24].

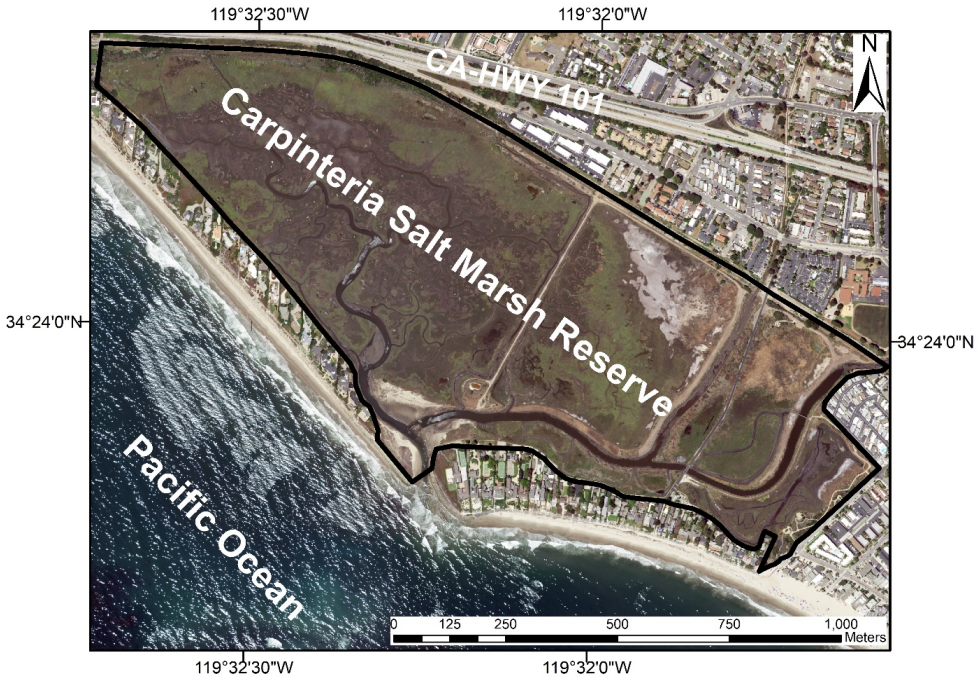

Figure 1. Carpinteria Salt Marsh Reserve with study extent outlined. Imagery courtesy of USDA National Agriculture Inventory Program.

2.2. Data Description and Correction

The imagery used in this study is Sentinel-2 A and B data produced by the European Space Agency. The mission is composed of two multispectral satellites that collect images that cover a large spatial extent, have a fine spatial resolution (up to 10 m for half the electromagnetic bands they detect), and a five day revisit time using both sensors. Both

satellites carry optical sensors that sample in 13 spectral bands at varying spatial resolutions (Table 1) [25,26]. The high temporal resolution of the two satellites allowed us to assemble a time series for quantifying marsh change despite the variable cloud cover and inundation of CSMR which would prevent accurate image analysis. Imagery dates were selected to represent similar times of year, tide, and cloud cover. Four dates were selected to establish pre-flow, immediate, and post-flow conditions (approximately one and three years after the initial Montecito Debris Flows). Imagery from 13 November 2017 was used for pre-flow conditions as it was the date closest to the debris flow in which the marsh was not flooded or covered by clouds. Imagery from 12 January 2018 represented the immediate conditions as the data were collected three days after the flow occurred and before mechanical clean up and king tides occurred. Lastly, 3 November 2018 and 12 November 2020 imagery represented two recovery steps and were chosen to be consistent with the pre-flow November image. No November 2019 imagery was selected, as all available images were collected when there was either dense cloud cover or the marsh was inundated by high tide. All Sentinel-2 imagery was downloaded from the USGS Earth Explorer portal [27].

Table 1. Sentinel-2 band descriptions.

Band	Resolution (m)	Central Wavelength (nm)	Bandwidth (nm)	Description
B1	60	443	21	Ultra blue (Coastal and Aerosol)
B2	10	490	66	Blue
B3	10	560	36	Green
B4	10	665	31	Red
B5	20	705	15	Visible and Near Infrared (VNIR)
B6	20	740	15	Visible and Near Infrared (VNIR)
B7	20	783	20	Visible and Near Infrared (VNIR)
B8	10	842	106	Visible and Near Infrared (VNIR)
B8a	20	865	21	Visible and Near Infrared (VNIR)
B9	60	940	20	Short Wave Infrared (SWIR)
B10	60	1375	31	Short Wave Infrared (SWIR)
B11	20	1610	91	Short Wave Infrared (SWIR)
B12	20	2190	175	Short Wave Infrared (SWIR)

Imagery was preprocessed in the Sentinel Application Platform (SNAP) prior to being implemented in ENVI Classic 5.5.3 [28,29]. First, the Sen2Cor SNAP add-on was used to perform atmospheric correction to obtain bottom of atmosphere L2A imagery from the top of atmosphere L1C imagery downloaded from the USGS [30]. This process produced 12 atmospherically-corrected L2A bands. Once corrected, bands 1, 9, and 10 were removed as they are primarily used for atmospheric properties and are too coarse (60 m resolution) to be used in assessment of the fine scale change in the marsh. The remaining 20 m resolution bands (bands 5, 6, 7, 8A, 11, and 12) were then resampled using pixel replication to match the 10 m resolution of bands 2, 3, 4, and 8. Resampled and native 10 m resolution bands were layer stacked for further processing in ENVI.

High density LiDAR was also used in addition to Sentinel-2 imagery to assess conditions immediately after the debris flows occurred (January 2018). The LiDAR data were collected over the areas affected by the debris flows soon after the event by the Federal Emergency Management Agency (FEMA) at a density of at least 4 points per square meter [31]. LiDAR data were corrected and processed using the BCAL add-on for ENVI [29,32]. Data were height filtered at a threshold of 30 m with a 10 m search window. Height filtered

data were then processed using last returns into a digital terrain model (DTM) with 10 m resolution to match Sentinel-2 data.

2.3. Spectral Analysis

Before classification, corrected Sentinel-2 images were processed to obtain fractional cover and to calculate the normalized difference vegetation index (NDVI) and modified anthocyanin reflectance index (mARI).

Fractional cover was obtained via MESMA using the following steps. First, two spectral libraries were generated using the November 2017 and January 2018 processed images. Endmembers were selected based on site knowledge and similarity of spectra to those that would be expected for each landcover class (November endmember spectra are shown in Figure 2). Both libraries had endmembers selected to represent four broad landcovers that are expected in the marsh: non-photosynthetic vegetation (NPV), green vegetation, bare soil, and subtidal (water). Libraries were optimized using the endmember average root mean square error (RMSE) (EAR) [33], minimum average spectral angle (MASA) [34] and count-based endmember selection (CoB) [35], or the EMC option in VIPER Tools, and included a minimum of four sample endmembers per landcover class [36]. The November library was used for the pre-debris and two recovery images. The January 2018 image had a separate spectral library for the unique conditions that were expected around the debris flow.

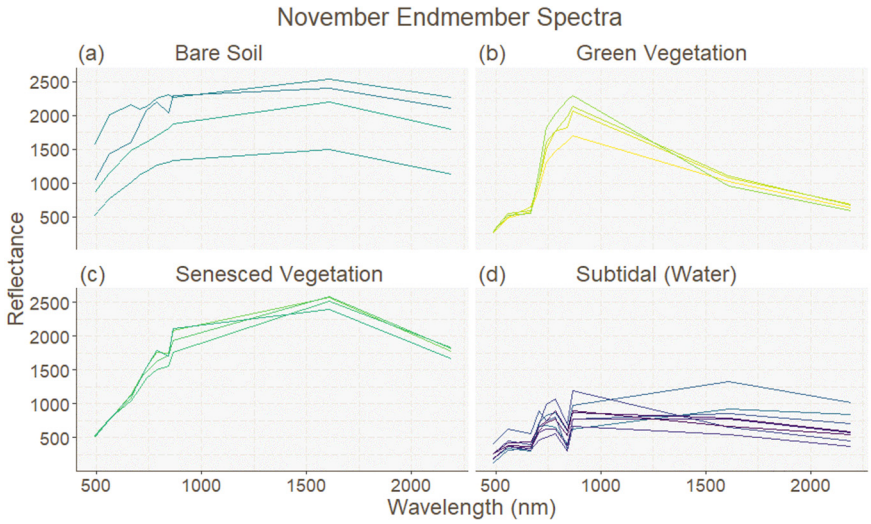

Figure 2. Spectral library for November 2017. Axes are (*x*-axis) wavelength in nm and (*y*-axis) reflectance values. Spectral signatures for (**a**) bare soil, (**b**) green vegetation, (**c**) non-photosynthetic vegetation (senesced), and (**d**) subtidal cover classes. Colors used for visual differentiation of the different endmembers.

With the libraries generated, MESMA was performed to obtain fractional cover for all four dates. Endmember models used were 2-, 3-, 4-, and 5-endmember models to ensure the inclusion of the model approaches recommended by Rosso et al. (2005) [12]. All models were constrained to fractional cover between 0.0 and 1.0, shade fraction between 0.0 and 0.8, and a maximum RMSE of 0.025. This process produced fractional cover for the four endmember classes for each date (Figure 3 for example).

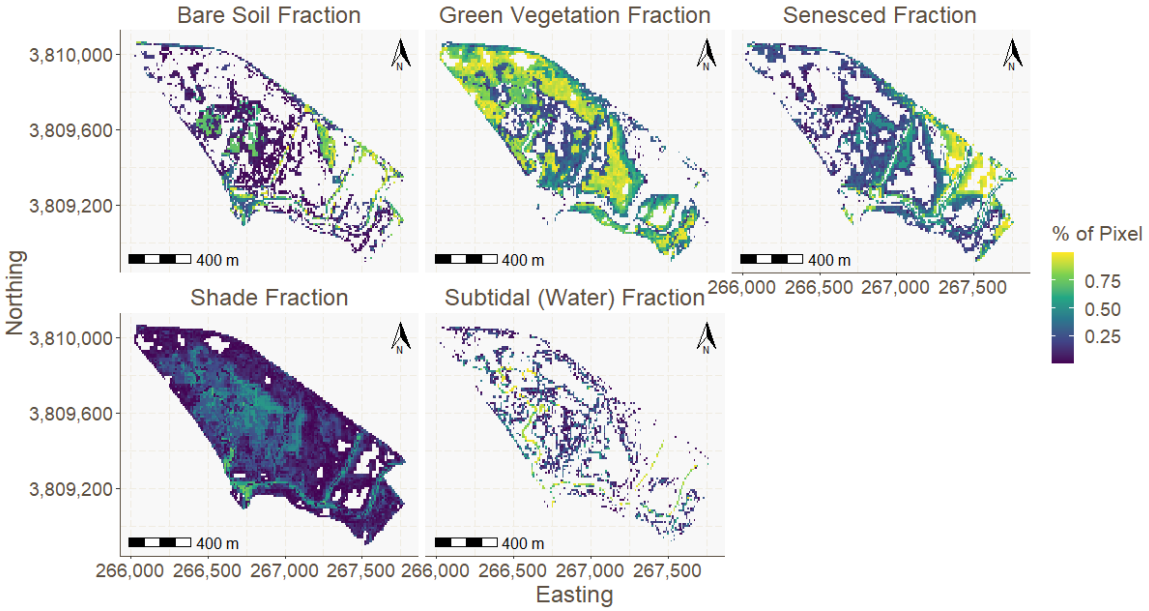

Figure 3. Fractional cover for November 2020 shown as an example of MESMA results. Scale indicates proportion of pixel that is made up of respective endmembers or shade. Pixels with a 0% cover were removed for visual clarity.

To further build on the data that would guide the classification of CSMR, two vegetation indices were calculated from the Sentinel-2 imagery: NDVI (Equation (1)) [37] and mARI (Equation (2)) [38,39].

$$\text{NDVI} = \frac{(NIR - RED)}{(NIR + RED)} = \frac{(Band8 - Band4)}{(Band8 + Band4)}, \quad (1)$$

NDVI is one of the vegetation indices recommended in the literature for wetland analysis and was found to be one of the more important factors in classifying landcover classes in CSMR in prior work [6,9,10,19].

$$\text{mARI} = 800\ \text{nm} \cdot \left(\frac{1}{550\ \text{nm}} - \frac{1}{700\ \text{nm}}\right) = Band8 \cdot \left(\frac{1}{Band3} - \frac{1}{Band5}\right), \quad (2)$$

mARI is used to detect the levels of anthocyanins, a family of red pigments that can be related to stress and senescence in plants [40]. Anthocyanin content in *Salicornia pacifica* has been found to increase in the fall and winter [41]. Therefore, mARI has the potential to further help the classification of both senesced vegetation and a dominant marsh plant in CSMR.

Once the Sentinel-2 and LiDAR products were produced, data were layer stacked prior to the creation of training data. Training data were produced for five landcover classes—bare soil, high marsh, mid marsh, senesced, and subtidal—by selecting reference polygons that matched regions of corresponding landcover from an expert map and from a report of landcover prior to the debris flow developed by Myers et al. (2017) (see Table 2) [23]. The high marsh class represents a mixed plant community of *Salicornia pacifica*, *Arthrocnemum subterminale*, *Frankenia salina*, and *Distichlis spicata*. Mid marsh represents portions of the marsh dominated by *S. pacifica*. The senesced landcover is composed of upland regions dominated by non-native shrubs and grasses [23]. Training data were collected for each date by creation of rectangular polygons in ArcGIS (Table 2 and Supplementary Materials Table S1) [42]. Training data and layer stacked images were analyzed in R [43].

Table 2. Polygon counts and decision metrics for training data generation.

Polygon Counts					
Class	**November 2017**	**January 2018**	**November 2018**	**November 2020**	**Metric**
Bare soil	10	11	17	13	High Bare Soil Fractions, Low NDVI, Low mARI
High Marsh	5	5	10	7	High Green Vegetation Fraction, High NDVI, High mARI
Mid Marsh	12	7	16	13	Moderate-High NDVI, Mixed Green Vegetation Fractions and Bare Soil Fractions
Senesced	8	5	8	5	High Non-photosynthetic Vegetation Fractions, Low NDVI, High mARI
Subtidal	20	7	21	19	High Subtidal Fractions, Low NDVI

2.4. Random Forest and Change Detection

We used a random forest classifier to assign landcover class to each pixel. Random forest is a machine learning technique that automates the categorization of data by running a datapoint (e.g., a pixel) through a set number of decision trees and picking a finalized landcover class via majority vote. Pixel values were first extracted from the layer stacked images with the values and associated landcover recorded into a data frame, which was then filtered to remove variables with NA/NULL values. The data frame was then read into the random forest algorithm, with n = 500 decision trees. This process produced classified maps of the five landcover classes. Additional outputs include: (1) variable importance, a measure that identifies which layer stack inputs were important in the landcover classification; (2) mtry accuracy, an accuracy assessment metric of the final model; and (3) kappa values, a secondary accuracy assessment metric. Final model selection and accuracy assessment were done via k-fold cross validation. Post-classification change detection was performed in ENVI using the change detection statistics option. Dates were compared to each other in both chronological order (i.e., November 2017 to January 2018, November 2018 to November 2020) and net order (November 2017 to November 2020). Comparing the dates this way allowed us to track landcover and to obtain extent for all five classes as time progressed, thus obtaining net change for each landcover class in the system. ENVI reported change statistics in terms of pixel count, area in square meters, and percentage change. These statistics include class differences and image differences. Percentage change was recalculated using both pixel count and area and used in place of the ENVI reported percentages.

3. Results

3.1. Random Forest

Variable importance was used to determine which of the random forest inputs were most important in the landcover classification of CSMR. Variable importance was measured by the mean decrease in Gini index (Gini value), a measure in which higher values indicate higher importance in the model (Table 3) [44]. From this measure, NDVI and green vegetation fraction were the most important variables in three of the four years. NDVI and green vegetation fractions did not have the highest importance in January 2018 and November 2020, respectively. Secondary variables that also had high importance were mARI, bare soil fractions, and senesced vegetation. Recovery time steps had greater mARI importance compared to the earlier dates. Shade fractions and subtidal fractions had the lowest amount of importance in many of the dates. The bare surface model (digital elevation) was only available and used for January 2018 but had moderate importance in

the model. LiDAR was not used for other dates due to expected differences in surface from time of the debris flow to later dates. Additionally, January 2018 had the lowest values for decrease in Gini index, and this could be linked to having more variables to use and/or high solar zenith angle.

Table 3. Variable importance across dates (mean decrease in Gini index).

Date	Soil Fraction	Green Veg Fraction	Senesced Fraction	Subtidal Fraction	Shade Fraction	NDVI	mARI	Digital Terrain
November 2020	62.24	58.33	45.79	31.21	46.56	109.52	99.69	
November 2018	55.01	63.01	25.91	50.83	20.55	60.63	17.14	
January 2018	31.07	43.72	41.79	28.53	8.96	17.28	4.87	23.17
November 2017	40.61	94.05	60.13	23.08	34.99	83.23	21.95	

Final model selection was done via k-fold cross validation where models with the lowest error were selected as the final model, with accuracies being reported for each number of splits tested. The number of splits that occur at each node within a decision tree is indicated by mtry; the random forest model then selects the mtry with the highest accuracy as the final prediction. The final mtry accuracy values (mtry = 2, 8, 2, and 2 respectively, Table 4) were high for all four dates—99.5%, 93%, 95.6%, and 97.1%, respectively—with similar kappa values—99.3%, 91.1%, 94.3%, and 96.3%.

Table 4. Class error and final model accuracy across dates.

Class	November 2017		January 2018		November 2018		November 2020	
	User's Error	Producer's Error	User's Error	Producer's Error	User's Error	Producer's Error	User's Error	Producer's Error
Bare Soil	0.103	0.062	0.038	0.05	0.020	0	0.061	0.013
High Marsh	0	0	0.017	0.048	0	0	0.006	0.011
Mid Marsh	0.030	0.072	0.171	0.105	0	0.024	0.071	0.064
Senesced Veg.	0.019	0.088	0	0	0.018	0	0	0.009
Subtidal/Water	0.12	0.029	0.1	0.1	0	0	0.061	0.089
	Accuracy	Kappa	Accuracy	Kappa	Accuracy	Kappa	Accuracy	Kappa
Final Model Accuracy	0.995	0.993	0.930	0.911	0.956	0.943	0.971	0.963

Landcover class accuracy was measured via producer's and user's error and allows for the assessment of the mapping of individual landcover classes (Table 4). High marsh vegetation was most accurately mapped with low user's and producer's error across all dates. Subtidal and mid marsh had the greatest amount of user's and producer's error, especially in January 2018. Subtidal cover had the greatest confusion with mid marsh vegetation and bare soil, while mid marsh was confused with bare soil and subtidal. Error within the subtidal and mid marsh classes was below 10% for most dates, and classification for the two classes remained relatively accurate.

3.2. Post-Classification Change Detection

The random forest classifier produced four landcover maps for CSMR (Figure 4). Each map shows the extent of the five landcover classes—bare soil, high marsh, mid marsh, senesced, and subtidal—and represents different states of disturbance and recovery. The high marsh landcover had the most area in November 2017 and January 2018, and mid marsh vegetation was the largest landcover class in November 2018 and 2020 (Figures 5

and 6). Senesced vegetation and subtidal landcover experienced little change compared to bare soil, high marsh, and mid marsh vegetation (Figures 5 and 6).

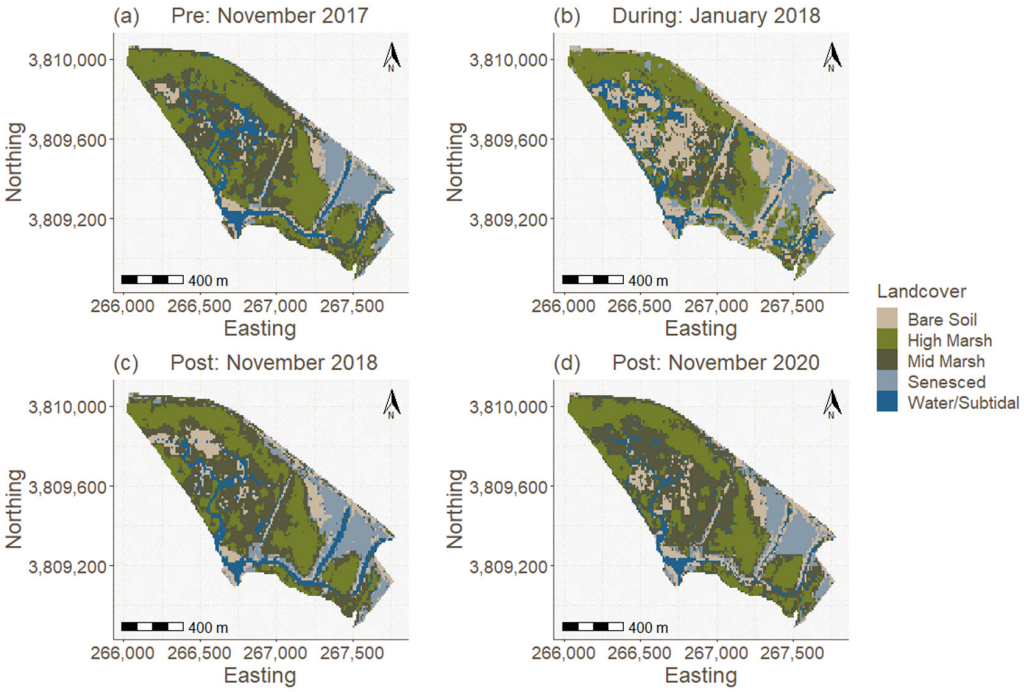

Figure 4. Maps produced by the random forest classification. Maps depict the extent of bare soil, high marsh, mid marsh, senesced vegetation, and subtidal/water landcover. Top to bottom, left to right: (**a**) November 2017, (**b**) January 2018, (**c**) November 2018, and (**d**) November 2020. (Projection: NAD 84 UTM Zone 11).

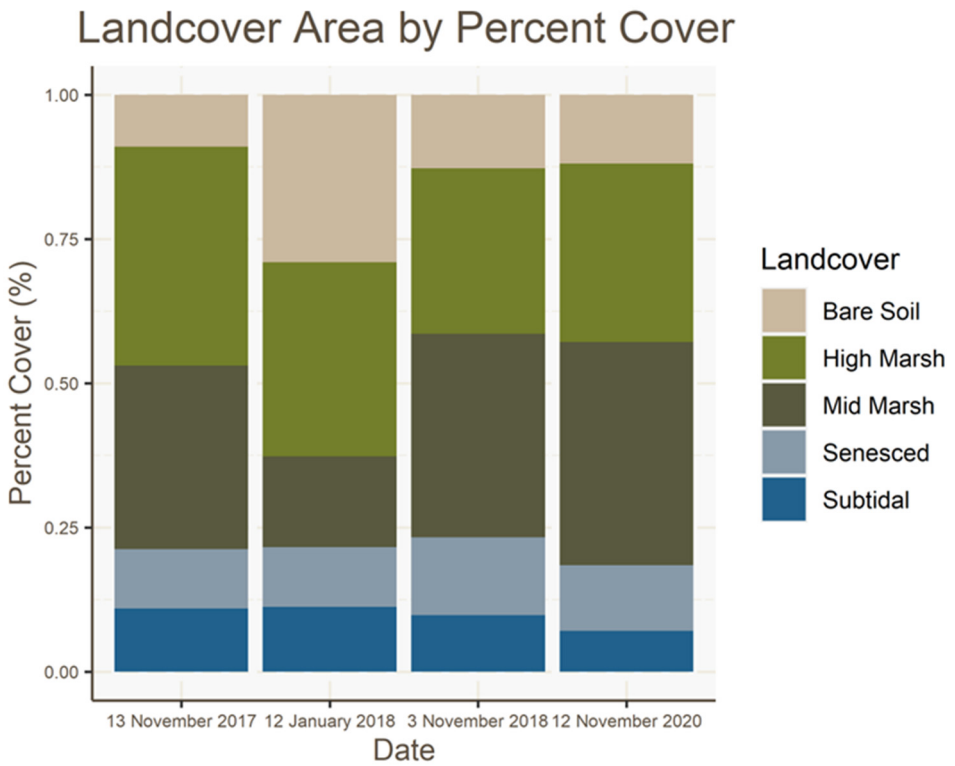

Figure 5. Percent cover for each landcover class in CSMR stacked by date.

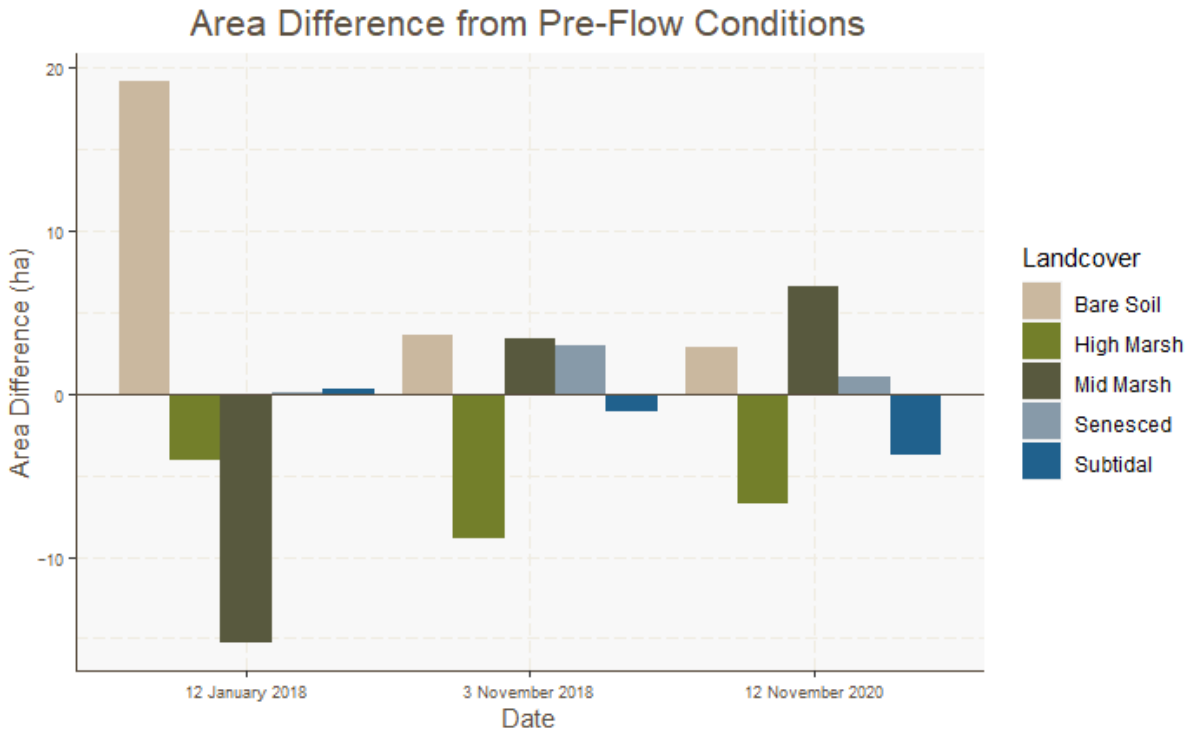

Figure 6. Difference of landcover class area (ha) compared to pre-flow conditions (November 2017). Bars are clustered by date.

The post-classification change detection showed a 19.1 ha increase in bare soil coverage between November 2017 and January 2018 (Figure 6). This amounted to 27.69 ha (~29%) of the marsh being covered in bare soil immediately following the debris flow (Figure 5). In November 2020, bare soil coverage decreased by 15.52 ha when compared to January 2018, a decrease of bare soil coverage to 12.17 ha (~16%) of total marsh area (Figure 5). Between November 2017 and November 2020, there was a 2.66 ha (~31%) net increase in bare soil coverage in the marsh (Figure 6).

On the other hand, overall marsh vegetation (high marsh + mid marsh) coverage experienced little change, with only a 0.1 ha (0.15%) net decrease in total vegetation coverage between November 2017 and November 2020 (Figure 5). However, when split into the two respective vegetation landcover classes, we find that high marsh vegetation coverage decreased as mid marsh vegetation increased (Figure 6). There were a few areas where change in landcover was prominently seen in the landscape, especially areas that were high marsh vegetation and/or near areas covered by bare soil that changed to mid marsh vegetation, such as near the salt pan in the northeast (Figure 7c) and some of the mudflat region in the western portion of the marsh (Figure 7a,b).

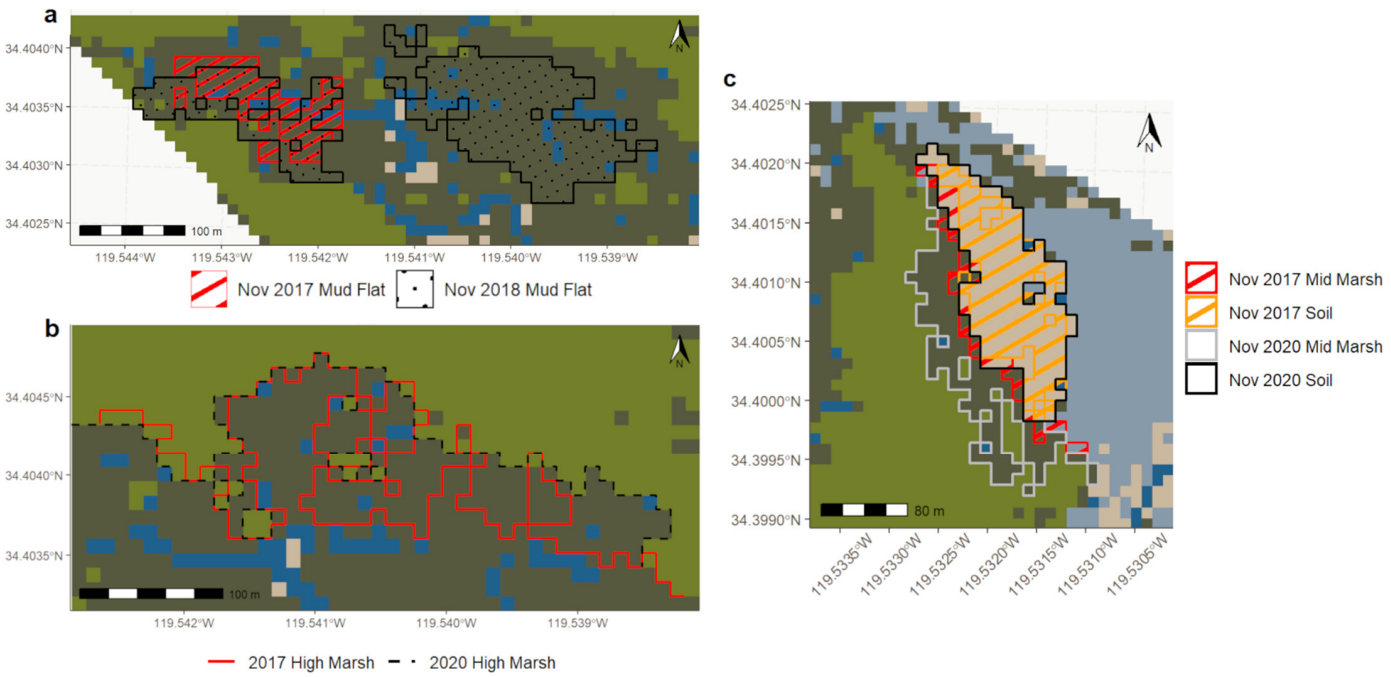

Figure 7. Maps highlighting areas where landcover change is most prominent. (**a**) High marsh to mid marsh conversion, (**b**) difference in mudflat extent, and (**c**) difference in salt pan (soil) and vegetated (mid marsh) perimeter. (Projection: NAD 84 UTM Zone 11, converted to lat/long).

4. Discussion

4.1. Model Accuracy

The accuracy metrics (mtry accuracy, kappa, producer's and user's error) suggested that landcover was accurately mapped by the random forest classifier and that the produced maps were reliable for use in change detection. The accuracy of the random forest classification is comparable to that of other wetland classifications. For example, Wu et al. (2020) also performed a random forest classification for a subtropical wetland that had a similar overall accuracy value of 92.96% compared to this study's average of 96.3% [17]. The model also performed as well as or better than classifications done using other methods such as maximum likelihood classification, iso-cluster unsupervised classification, or reclassification/recoding of vegetation indices [14,16,19]. The random forest classification done here was more accurate than the maximum likelihood classification done by Parihar et al. (2012), with an average accuracy of 96.3% vs. 76.5%, respectively [14]. When compared to Tuxen et al. (2007), the random forest did approximately the same or slightly better than reclassification, with reclassification having accuracy values of 81.4% and 96.3% compared to our average accuracy of 96.3% [19]. Iso-cluster classification on NDVI did somewhat better than the random forest, with accuracy values of 97.3%, 97.5%, 97.6%, and 98.0% for the respective dates [16].

High marsh had the highest accuracy, while the mid marsh class had high user's and producer's errors. As mid marsh is one of the classes that experienced the most change following the debris flow, any error present in its classification presents a problem; however, this error only exceeds 10% in January 2018 (user's: 17.1%, producer's: 10.5%) and is within acceptable margins for all other dates. Possible sources for the error include: (1) training data may have included misclassified pixels and introduced error to the corresponding landcover class, (2) pixels may have had values similar to that of multiple landcover classes, (3) resampled 20 m resolution Sentinel-2 bands may have still been too coarse to assess changes in the marsh, and (4) the use of a different spectral library for January 2018 may have led to lower accuracies for this date. To remedy this, the use of data from higher spatial resolution sensors may be useful in reducing the frequency of mixed pixels and the need for fractional cover. Additionally, higher spectral resolution may improve the building

of spectral libraries that can better differentiate between endmember classes, which then improves inputs into the random forest model.

4.2. Landcover Change and Ecological Implications

A majority of the landcover change occurred in bare soil, high marsh, and mid marsh vegetation. Bare soil area increased by 222% following the debris flows and dropped considerably in area by November 2018, likely due to the mechanical clean-up effort and king tides which removed a large amount of the sediment. Bare soil continued to decrease until there was only a net 31% increase in bare soil by November 2020. This may indicate that the marsh was still recovering from the debris flows and would continue to change over time.

Total vegetated area in the marsh showed little change over the 3 years, with only a 0.15% decrease in total marsh vegetation between November 2017 and November 2020. However, change was occurring, which is apparent when total vegetation is broken down into community types (high vs. mid marsh) and compared. High marsh (a mixed community of *Salicornia pacifica*, *Arthrocnemum subterminale*, *Frankenia salina*, and *Distichlis spicata*) area decreased by about the same amount that mid marsh (primarily only *S. pacifica*) area increased, creating the illusion of little change in vegetated area. The post-classification change detection showed that this shift from high to mid marsh community primarily occurred near areas that had been covered by bare soil following the debris flow.

The conversion to mid marsh vegetation from high marsh vegetation signifies a decrease in plant biodiversity as the community shifts from a mixed community to one that is largely composed solely of *S. pacifica*. This change in diversity poses some ecological challenges important to long-term wetland management. Studies have shown that a less diverse community is less resilient to the effects of disturbance, and spatial heterogeneity is important in the enhancement of the resilience of ecosystem functions [45]. Less resilience may dictate a need for more management intervention following disturbances, especially as the frequency of disturbances, such as wildfire, sea level rise and flooding, and landslide and mudslide damage, are predicted to increase with global climate change [7]. Studies have found that the addition of sediment via depositional events can promote plant growth by the delivery of mineral nutrients [5]. These nutrients may promote increased primary productivity by providing limiting nutrients. However, biodiversity has also been found to be positively linked to primary productivity and its temporal stability [46]. A trend of conversion from a mixed community of several plant species to one made of primarily only one plant species may have harmful repercussions for marsh productivity and other ecosystem services and functions. Determining whether this change to a less diverse community is a permanent change or only a short-term condition as the marsh recovers from the debris flow would require analysis of a longer time series of imagery over several years following the debris flows.

Sea level rise (SLR) is a challenge for the conservation of coastal wetlands, especially in developed regions, as rising sea levels contribute to coastal squeeze, leading to landcover change, fragmentation, and eventual loss of coastal marshes [47]. Sediment deposition and soil accretion are viewed as important processes for the offsetting of SLR [5,48]. However, our results imply that debris flow deposition is also leading to landcover and plant community change. While there are not clear policy implications from this work, beyond possibly assisted restoration, landcover change may become an important consideration when planning for the management of coastal wetlands that can be prone to depositional events; this study is an important example of how to inform those plans in the absence of field data.

4.3. Limitations and Challenges

As discussed above, the resolution of remotely sensed data is important in the assessment of the fine scale changes that occur in marsh ecosystems. Some Sentinel-2 bands do not have a native 10 m resolution and, therefore, have pixels that represent an average

of a larger mix of landcover types. Resampling, as conducted in this study, only splits this coarser data into smaller pixels and not into its disaggregated components. Therefore, landcover classification would benefit from a sensor where all bands have the same fine spatial resolution, such as unmanned aerial vehicles. High density LiDAR for more dates would also help in the assessment of biomass and vertical landcover differences such as water in channels vs. plants in upland regions. In addition, the baseline landcover prior to the debris flow was limited to a single date due to cloud cover, tide, and the length of historical record. Baseline assessments could be improved by using a sensor with a longer history or by using multiple dates per year. Ground reference data were also scarcely available due to the lack of prior field data to compare against classification of historical imagery and due to the COVID-19 pandemic limiting ability to go into the field to collect such data, hence the emphasis on other accuracy metrics. The results are also limited in their predictive power. For example, the rate at which sediment is being removed from the system or identification of whether the recently mapped sediment was the same sediment that had been deposited during the debris flow cannot be properly ascertained from these data. The processes leading to the conversion of high marsh to mid marsh vegetation also cannot be directly detected from these data.

5. Conclusions

Post-classification change detection tracked change in the five different landcover types in CSMR and found that mid marsh, high marsh, and bare soil landcover changed most dramatically in the dates studied. Total marsh vegetation (high marsh + mid marsh) cover returned to similar levels to those before the debris flows; however, assessing change as total marsh vegetation, as was the initial frame of the research question, does not lead to a robust conclusion. Areas that were covered in debris transitioned from high marsh vegetation to mid marsh vegetation despite total vegetated area remaining relatively unchanged. This transition has important ecological implications for marsh productivity and resilience to disturbance that continue after the debris is removed from the system.

The method used here shows promise in being applied to other depositional disturbances to wetland systems. For example, the random forest model identified important classification variables that can be used to classify marsh landcover without field-based data. The method can also serve as an important first step in the identification of regions of interest that can be used to inform field campaigns to address further questions that arise from the use of remote sensing (e.g., a field campaign to assess the factors that are leading to the transition from high marsh to mid marsh vegetation).

The Montecito Debris Flows provided a unique opportunity to study debris interactions with marshes in a context different than what is known from previous studies which more commonly focused on hurricane deposition. Data and information are an important part of making informed management decisions, and this study provides a successful demonstration of the use of post-classification change detection to assess wetland landcover response to an episodic event and the data that can be expected from such an assessment.

Supplementary Materials: The following supporting information can be downloaded at: https://www.mdpi.com/article/10.3390/rs14122819/s1, Table S1. Descriptive Statistics for Training Data Parameters, including min. and max. values, mean, and standard deviation for all variables used.

Author Contributions: G.D.S., D.A.R., J.P.M., and J.Y.K. contributed to study conception and design. Material preparation, data collection, and analyses were performed by G.D.S. The first draft of the manuscript was written by G.D.S., and all authors commented on previous versions of the manuscript. All authors have read and agreed to the published version of the manuscript.

Funding: This work was supported by the National Science Foundation Graduate Research Fellowship to GDS (Grant number: 2139319).

Data Availability Statement: Original Sentinel-2 data obtained from USGS Earth Explorer, available here: https://earthexplorer.usgs.gov/ (accessed on 2 February 2021). Code and end products

generated during this study, such as layered images, classified maps, etc., available here: https://github.com/German-Sil/carpinteria_debris_thesis (accessed on 10 November 2021).

Acknowledgments: The authors would like to acknowledge a few individuals and organizations: First, Kristin Morell for providing the FEMA LiDAR data set used in the January 2018 assessment and Andy Brooks for providing helpful insight into the landscape and work being done at Carpinteria Salt Marsh Reserve. Second, Alex Feldwinn for his computer support through the duration of the pandemic. And last, but certainly not least, the National Science Foundation Graduate Research Fellowship Program for funding the graduate work of G.D.S. that this manuscript is derived from.

Conflicts of Interest: The authors declare no conflict of interest. The funder had no role in the design of the study; in the collection, analyses, or interpretation of data; in the writing of the manuscript, or in the decision to publish the results.

References

1. Gibbs, J.P. Wetland Loss and Biodiversity Conservation. *Conserv. Biol.* **2000**, *14*, 314–317. [CrossRef]
2. Callaway, J.C.; Borgnis, E.L.; Turner, R.E.; Milan, C.S. Carbon Sequestration and Sediment Accretion in San Francisco Bay Tidal Wetlands. *Estuaries Coast* **2012**, *35*, 1163–1181. [CrossRef]
3. California Department of Fish and Wildlife. Coastal Wetlands-Emergent Marshes. California's Living Marine Resources: A Status Report. 2001. Available online: https://nrm.dfg.ca.gov/FileHandler.ashx?DocumentID=34250 (accessed on 16 May 2021).
4. Uhrin, A.V.; Schellinger, J. Marine Debris Impacts to a Tidal Fringing-Marsh in North Carolina. *Mar. Pollut. Bull.* **2011**, *62*, 2605–2610. [CrossRef] [PubMed]
5. Tweel, A.W.; Turner, R.E. Landscape-Scale Analysis of Wetland Sediment Deposition from Four Tropical Cyclone Events. *PLoS ONE* **2012**, *7*, e50528. [CrossRef] [PubMed]
6. Doughty, C.L.; Cavanaugh, K.C. Mapping Coastal Wetland Biomass from High Resolution Unmanned Aerial Vehicle (UAV) Imagery. *Remote Sens.* **2019**, *11*, 540. [CrossRef]
7. Erwin, K. Wetlands and Global Climate Change: The Role of Wetland Restoration in a Changing World. *Wetl. Ecol. Manag.* **2009**, *17*, 71–84. [CrossRef]
8. Beland, M.; Biggs, T.; Roberts, D.; Peterson, S.; Koklay, R.; Piazza, S. Oiling Accelerates Loss of Salt Marshes, Southeastern Louisiana. *PLoS ONE* **2017**, *12*, e0181197. [CrossRef]
9. Klemas, V. Remote Sensing of Coastal Wetland Biomass: An Overview. *J. Coast. Res.* **2013**, *29*, 1016–1028. [CrossRef]
10. Klemas, V. Remote Sensing of Emergent and Submerged Wetlands: An Overview. *Int. J. Remote Sens.* **2013**, *34*, 6286–6320. [CrossRef]
11. Peterson, S.H.; Roberts, D.A.; Beland, M.; Kokaly, R.F.; Ustin, S.L. Oil Detection in the Coastal Marshes of Louisiana Using MESMA Applied to Band Subsets of AVIRIS. *Remote Sens. Environ.* **2015**, *159*, 222–231. [CrossRef]
12. Rosso, P.H.; Ustin, S.L.; Hastings, A. Mapping Marshland Vegetation of San Francisco Bay, California, Using Hyperspectral Data. *Int. J. Remote Sens.* **2005**, *26*, 5169–5191. [CrossRef]
13. Eastwood, J.A.; Yates, M.G.; Thomson, A.G.; Fuller, R.M. The Reliability of Vegetation Indices for Monitoring Saltmarsh Vegetation Cover. *Int. J. Remote Sens.* **1997**, *18*, 3901–3907. [CrossRef]
14. Parihar, S.M.; Sarkar, S.; Dutta, A.; Sharma, S.; Dutta, T. Characterizing Wetland Dynamics: A Post-Classification Change Detection Analysis of the East Kolkata Wetlands Using Open Source Satellite Data. *Geocarto Int.* **2013**, *28*, 273–287. [CrossRef]
15. Miller, G.J.; Morris, J.T.; Wang, C. Estimating Aboveground Biomass and Its Spatial Distribution in Coastal Wetlands Utilizing Planet Multispectral Imagery. *Remote Sens.* **2019**, *11*, 2020. [CrossRef]
16. Nasser Mohamed Eid, A.; Olatubara, C.O.; Ewemoje, T.A.; Farouk, H.; Talaat El-Hennawy, M. Coastal Wetland Vegetation Features and Digital Change Detection Mapping based on Remotely Sensed Imagery: El-Burullus Lake, Egypt. *Int. Soil Water Conserv. Res.* **2020**, *8*, 66–79. [CrossRef]
17. Wu, L.; Li, Z.; Liu, X.; Zhu, L.; Tang, Y.; Zhang, B.; Xu, B.; Liu, M.; Meng, Y.; Liu, B. Multi-Type Forest Change Detection Using BFAST and Monthly Landsat Time Series for Monitoring Spatiotemporal Dynamics of Forests in Subtropical Wetland. *Remote Sens.* **2020**, *12*, 341. [CrossRef]
18. Roberts, D.A.; Gardner, M.; Church, R.; Ustin, S.; Scheer, G.; Green, R.O. Mapping Chaparral in the Santa Monica Mountains Using Multiple Endmember Spectral Mixture Models. *Remote Sens. Environ.* **1998**, *65*, 267–279. [CrossRef]
19. Tuxen, K.; Schile, L.; Kelly, M.; Siegel, S. Vegetation Colonization in a Restoring Tidal Marsh: A Remote Sensing Approach. *Restor. Ecol.* **2008**, *16*, 313–323. [CrossRef]
20. Im, J.; Jensen, J.R.; Hodgson, M. Object-Based Land Cover Classification Using High-Posting-Density LiDAR Data. *GISci. Remote Sens.* **2008**, *45*, 209–228. [CrossRef]
21. Andone, D. The Largest Wildfire in California's Modern History is Finally Out, More Than 6 Months After It Started. CNN. Cable News Network. 2018. Available online: https://www.cnn.com/2018/06/02/us/thomas-fire-officially-out/index.html (accessed on 16 May 2021).

22. Kean, J.W.; Staley, D.M.; Lancaster, J.T.; Rengers, F.K.; Swanson, B.J.; Coe, J.A.; Hernandez, J.L.; Sigman, A.J.; Allstadt, K.E.; Lindsay, D.N. Inundation, Flow Dynamics, and Damage in the 9 January 2018 Montecito Debris-Flow Event, California, USA: Opportunities and Challenges for Post-Wildfire Risk Assessment. *Geosphere* **2019**, *15*, 1140–1163. [CrossRef]
23. Myers, M.R.; Cayan, D.R.; Iacobellis, S.F.; Melack, J.M.; Beighley, R.E.; Barnard, P.L.; Dugan, J.E.; Page, H.M. Santa Barbara Area Coastal Ecosystem Vulnerability Assessment. CASG-17-009 2017. California. Available online: https://caseagrant.ucsd.edu/sites/default/files/SBA-CEVA-final-0917.pdf (accessed on 13 January 2021).
24. Brooks, A. (University of California, Santa Barbara, Santa Barbara, CA, USA). Personal communication, 2019.
25. Drusch, M.; Del Bello, U.; Carlier, S.; Colin, O.; Fernandez, V.; Gascon, F.; Hoersch, B.; Isola, C.; Laberinti, P.; Martimort, P.; et al. Sentinel-2: ESA's Optical High-Resolution Mission for GMES Operational Services. *Remote Sens. Environ.* **2012**, *120*, 25–36. [CrossRef]
26. European Space Agency. Overview—Sentinel Online. Available online: https://sentinel.esa.int/web/sentinel/missions/sentinel-2/overview (accessed on 16 May 2021).
27. U.S. Geological Survey. Earth Explorer. Geological Survey (U.S.) FS 083-00. 2000. Available online: https://earthexplorer.usgs.gov/ (accessed on 15 November 2020).
28. SNAP—ESA Sentinel Application Platform v8.0. Available online: https://step.esa.int (accessed on 15 November 2020).
29. Harris Geospatial. *Exelis Visual Information Solutions*; Harris Geospatial: Boulder, CO, USA, 2013. Available online: https://www.l3harrisgeospatial.com/ (accessed on 15 November 2020).
30. Main-Knorn, M.; Pflug, B.; Louis, J.; Debaecker, V.; Müller-Wilm, U.; Gascon, F. Sen2Cor for Sentinel-2. *Proc. SPIE* **2017**, *10427*, 1042704. [CrossRef]
31. Federal Emergency Management Agency. *Montecito Debris Flow LiDAR*; Federal Emergency Management Agency: San Francisco, CA, USA, 2018.
32. Streutker, D.R.; Glenn, N.F. LiDAR Measurement of Sagebrush Steppe Vegetation Heights. *Remote Sens. Environ.* **2006**, *102*, 135–145. [CrossRef]
33. Dennison, P.E.; Roberts, D.A. Endmember Selection for Multiple Endmember Spectral Mixture Analysis using Endmember Average RSME. *Remote Sens. Environ.* **2003**, *87*, 123–135. [CrossRef]
34. Dennison, P.E.; Halligan, K.Q.; Roberts, D.A. A Comparison of Error Metrics and Constraints for Multiple Endmember Spectral Mixture Analysis and Spectral Angle Mapper. *Remote Sens. Environ.* **2004**, *93*, 359–367. [CrossRef]
35. Roberts, D.A.; Dennison, P.E.; Gardner, M.; Hetzel, Y.; Ustin, S.L.; Lee, C. Evaluation of the Potential of Hyperion for Fire Danger Assessment by Comparison to the Airborne Visible/Infrared Imaging Spectrometer. *IEEE Trans. Geosci. Remote Sens.* **2003**, *41*, 1297–1310. [CrossRef]
36. Roberts, D.; Halligan, K.; Dennison, P.; Dudley, K.; Somers, B.; Crabbé, A. VIPER Tools. 2019. Available online: https://drive.google.com/drive/folders/0B0zkcpjAaSqFbUVacVJCSURtSzQ (accessed on 15 November 2020).
37. Rouse, J.W.; Haas, H.R.; Deering, D.W.; Schell, J.A.; Harlan, J.C. *Monitoring the Vernal Advancement and Retrogradation (Green Wave Effect) of Natural Vegetation*; NASA/GSFC Type III Final Rep.; The Goddard Space Flight Center: Greenbelt, MD, USA, 1974; 371p.
38. Gitelson, A.A.; Keydan, G.P.; Merzlyak, M.N. Three-Band Model for Noninvasive Estimation of Chlorophyll Carotenoids and Anthocyanin Contents in Higher Plant Leaves. *Geophys. Res. Lett.* **2006**, *33*, L11402. [CrossRef]
39. Gitelson, A.A.; Chivkunova, O.B.; Merzlyak, M.N. Non-Destructive Estimation of Anthocyanins and Chlorophylls in Anthocyanic Leaves. *Am. J. Bot.* **2009**, *96*, 1861–1868. [CrossRef] [PubMed]
40. Gitelson, A.A.; Merzlyak, M.N.; Chivkunova, O.B. Optical Properties and Nondestructive Estimation of Anthocyanin Content in Plant Leaves. *Photochem. Photobiol.* **2001**, *74*, 38–45. [CrossRef]
41. Farrens, G. Color Change and Succulence in *Salicornia pacifica*. Master's Thesis, San Jose State University, San Jose, CA, USA, 1971.
42. Environmental Systems Research Institute. *ArcGIS. Version 10.7.1*; Environmental Systems Research Institute, Inc.: Redlands, CA, USA, 2019.
43. R Core Team. R: A Language and Environment for Statistical Computing; R Foundation for Statistical Computing, Vienna, Austria. 2019. Available online: https://www.R-project.org/ (accessed on 15 November 2020).
44. Lee, C. Feature Importance Measures for Tree Models—Part 1. 2017. Available online: https://medium.com/the-artificial-impostor/feature-importance-measures-for-tree-models-part-i-47f187c1a2c3 (accessed on 11 December 2020).
45. Oliver, T.H.; Heard, M.S.; Issac, N.J.B.; Roy, D.B.; Procter, D.; Eigenbrod, F.; Freckleton, R.; Hector, A.; Orme, C.D.L.; Petchey, O.L. Biodiversity and Resilience of Ecosystem Functions. *Trends Ecol. Evol.* **2015**, *30*, 673–684. [CrossRef]
46. Oehri, J.; Schmid, B.; Schaepman-Strub, G.; Niklaus, P.A. Biodiversity Promotes Primary Productivity and Growing Season Lengthening at the Landscape Scale. *Proc. Natl. Acad. Sci. USA* **2017**, *114*, 10160–10165. [CrossRef] [PubMed]
47. Torio, D.D.; Chmura, G.L. Assessing Coastal Squeeze of Tidal Wetlands. *J. Coast. Res.* **2013**, *29*, 1049–1061. [CrossRef]
48. Rosencranz, J.A.; Ganju, N.K.; Ambrose, R.F.; Brosnahan, S.M.; Dickhudt, P.J.; Guntenspergen, G.R.; MacDonald, G.M.; Takekawa, J.Y.; Thorne, K.M. Balanced Sediment Fluxes in Southern California's Mediterranean-Climate Zone Salt Marshes. *Estuaries Coast* **2016**, *39*, 1035–1049. [CrossRef]